Efficient rotor aerodynamics predictions with an Euler method

M.Biava[†], A.Pisoni[§], A.Saporiti[§], L.Vigevano[†]
[†] Dipartimento di Ingegneria Aerospaziale, Politecnico di Milano, Italy
[§] AGUSTA, Cascina Costa di Samarate (Varese), Italy

Abstract

The prediction of rotor loads in forward flight is carried out with the 3D unsteady Euler code ROSITA using a single-blade approach and accounting for the influence of the other blades by means of far-field boundary conditions. The latter are assigned by a free-wake vortex lattice code. Comparisons with experimental data and with computations obtained with other methods show that the single-blade approach may achieve accurate results, together with an improved efficiency with respect to multi-blade Chimera methods.

1 Introduction

The flow round helicopter rotor blades in forward flight is unsteady and characterized by strong non-linear and three dimensional effects, transonic regions near the tip of advancing blades, regions of shock induced separations and dynamic stall at retreating blades. In addition, the blades shed complex vortical wakes which strongly affects the operating characteristics of the rotor. Accurate predictions of the behavior of the trailing vortex generated at the blade tip are of paramount importance to rotor design. In hovering and descent flight the interaction between a blade and the tip vortex shed by the preceding blade is particularly intense and the blade vortex interaction (BVI) mechanism influences the blade loads and furthermore the impulse noise generated by the rotor itself.

Recent advances in modelling multi-bladed rotor flows have been made solving the Euler/Navier Stokes equations by the Chimera overlapping grid approach [1] - [4] , naturally suited for describing multiple bodies in relative motion. The Chimera philosophy was also adopted during the EC funded EROS project, the outcome of which was a common European rotorcraft aerodynamics simulation system [5], including both the GEROS grid generator and the EROS Euler solver. However, for a four- or five-blade rotor the computational effort required by a Chimera grid assembly may be so large to preclude obtaining fast predictions of the aerodynamic performances, needed during the preliminary design stage. A better computational efficiency may be achieved by solving for the near field of a *single* blade, providing the effects of the complete rotor wake system is properly taken into account. The methodology proposed here, similar to that experimented by Wagner and co-workers [6] , [7] , accounts for the coupling of a free-wake, unsteady vortex lattice model with the Euler solver [8]. The coupling is carried out by specifying as far-field condition for the Euler equations (fig. 1) the velocity field induced by the wake, initially computed with the help of the BEM code.

The present work aims at illustrating some of the forward flight results achieved by adopting the single-blade approach as implemented in the ROSITA code, an Agusta - Politecnico di Milano joint development of the EROS Euler solver.

2 Solver description

In order to achieve steady-state conditions in hovering and to ease the application of the Chimera methodology to multi-bladed rotors, the unsteady Euler equations in the ROSITA solver are formulated in terms of absolute velocity, expressed in a rotating frame of reference RF linked to each blade. The integral form of the equations may be written as:

$$\frac{d}{dt}\int_{\Omega} \boldsymbol{w} + \oint_{\partial\Omega} (\boldsymbol{f} - \boldsymbol{f}_e)\cdot\boldsymbol{n} = \int_{\Omega} \boldsymbol{s} \ ,$$

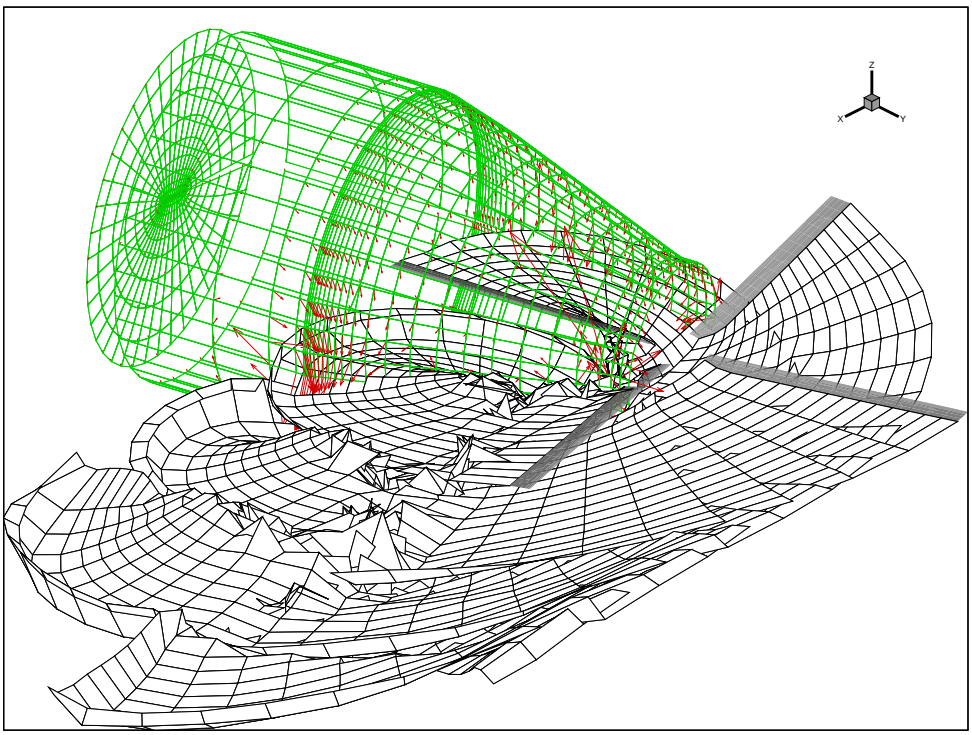

Figure 1: Single-blade approach.

where $\boldsymbol{n}$ is the outward normal vector and $\boldsymbol{w} = (\rho, \rho\boldsymbol{u}, E^{\mathrm{t}})^T$ is the conservative variable vector, with ρ mass density, $\boldsymbol{u}$ absolute velocity vector and E^{t} total energy per unit volume. The flux vectors and the source vector $\boldsymbol{s}$, arising from the non-inertial RF, are given by:

$$\boldsymbol{f} = \begin{pmatrix} \rho\boldsymbol{u}^T \\ \rho\boldsymbol{u}\boldsymbol{u} + P\boldsymbol{I} \\ (E^{\mathrm{t}} + P)\boldsymbol{u}^T \end{pmatrix}, \quad \boldsymbol{f}_e = \begin{pmatrix} \rho\boldsymbol{v}_e^T \\ \rho\boldsymbol{u}\boldsymbol{v}_e \\ E^{\mathrm{t}}\boldsymbol{v}_e^T \end{pmatrix},$$

$$\boldsymbol{s} = \begin{pmatrix} 0 \\ -\boldsymbol{\Omega} \times (\rho\boldsymbol{u}) \\ 0 \end{pmatrix},$$

where $\boldsymbol{v}_e$ is the entrainment velocity vector and $\boldsymbol{\Omega}$ the angular velocity vector of the RF in the absolute frame. All velocity vector components are expressed in the RF.

The above equations are discretized in space by means of a cell-centred finite-volume implementation of the Roe's scheme [9]. A high resolution scheme is obtained through the use of MUSCL extrapolation [10] supplemented with a total variation diminishing (TVD) limiter to ensure monotone solutions. The limiter formulation originally implemented in the EROS solver has been found to strongly influence the attainment of steady-state solutions in hover conditions [11]. Therefore it has been replaced by a modified version of the Van Albada limiter, proposed by Venkatakrishnan [12], depending from an empirical parameter K. A large value of K implies no limiting at all and therefore reduces the numerical diffusion of the scheme, but may lead to unstable solutions in case of shocked flows. Small values of K may improve the convergence to steady-state in hovering at the expense of degrading the accuracy.

Time advancement is carried out with a dual-time formulation [13]. A 2^{nd} order backward differentiation formula was applied to approximate the time derivative. An implicit scheme is used in pseudo-time , either a factored-unfactored (FUN) [14] or a recently implemented fully unfactored (UNFAC) method. The FUN method results in a two-factor linear system which can be loosely described as unfactored in each blade spanwise slice and approximately factored in spanwise direction. It therefore requires much less storage than the UNFAC method, at the expenses of a slower convergence to steady state and therefore of a reduced computational efficiency. Three-fold improvements of the speed of convergence to steady state has been obtained with UNFAC. Both algorithms use the generalized conjugate gradient (GCG) method to solve the resulting linear system, with preconditioning based on a block incomplete lower-upper (BILU) factorization.

The code has been fully parallelized using the MPI library to handle communications between processors. For parallel computations the grid is auto-

matically partitioned into several blocks during the preprocessing stage. The linear system stemming from the implicit scheme is solved separately for each block. The block connectivity boundary conditions are updated at each iteration of the GCG solver to retain the rate of convergence and the stability of the original single block scheme.

2.1 Wake calculation

To perform single-blade forward flight calculations with the Euler solver, the velocity induced by blades and wakes in correspondence of suitable points at the far field boundary are provided by the boundary element code NUVOLA, which is an unsteady, incompressible, inviscid, three dimensional vortex lattice method [15]. The blades are modelled as lifting surfaces, of zero thickness, based on the mean chord line of the airfoils with arbitrary twist and taper distribution. The discretization consists of quadrilateral elements with constant strength equal to the jump in the velocity potential. A time-marching free wake calculation is performed starting from an initial state of rest. At each time step a new row of wake panels is added at the trailing edge of each blade and the geometry of the wakes is updated according to the influence of all the other wakes and blades. A weak coupling is used to provide the far-field boundary conditions for the Euler code [8].

2.2 Vorticity confinement

The compressible vorticity confinement formulation requires the introduction of an additional term $\boldsymbol{f}_b$ in the momentum equation. The confinement term $\boldsymbol{f}_b$ may be written [16] in terms of a (constant) coefficient ϵ_c and of the vorticity $\boldsymbol{\omega}$ as:

$$\boldsymbol{f}_b = -\epsilon_c \boldsymbol{n}_c \times \boldsymbol{\omega},$$

with the vector $\boldsymbol{n}_c$ oriented in the direction opposite to the gradient of the vorticity magnitude:

$$\boldsymbol{n}_c = \frac{\boldsymbol{\nabla}|\boldsymbol{\omega}|}{|\boldsymbol{\nabla}|\boldsymbol{\omega}||}.$$

The source term $\boldsymbol{s}$ for the compressible confinement formulation is therefore modified as:

$$\boldsymbol{s} = \begin{pmatrix} 0 \\ -\boldsymbol{\Omega} \times (\rho \boldsymbol{u}) - \rho \epsilon_c \boldsymbol{n}_c \times \boldsymbol{\omega} \\ 0 \end{pmatrix}.$$

The inherent difficulty of this approach stems into the choice of the coefficient ϵ_c, that may vary of orders of magnitude for different flows [17].

3 Description of the test cases and computational details

The ONERA/ECF 7A and 7AD model rotors, tested at Modane and in the DNW tunnel during the HELISHAPE research campaign [18], were simulated. The 7A is a four-bladed rotor with 2.1 m radius, 0.14 m chord, linear twist distribution and rectangular planform. The blades have an aspect ratio of 15 and consists of airfoils of the OA2XX series with 13% to 9% thickness. The 7AD has similar dimension and airfoil shapes, but differs from 7A for the presence of a parabolic swept tip with anhedral angle.

In order to assess the accuracy of the proposed method we considered three Test Cases (TC). The first case refer to the 7AD rotor in high-speed, horizontal forward flight. The second and third cases consider the 7A rotor at low speed forward flight and descent flight, the latter exhibiting a stronger interaction between the blades and the wake system. The flight conditions reproduced in the experiments and in the computations are summarized in Table 1.

Two body fitted O-H grid were used for the Euler computations, made up, respectively, of $120 \times 50 \times 30$ cells (a "coarse" grid) and $150 \times 76 \times 45$ cells (a "medium" grid). In the wake calculations, the blade was approximated as a lifting surface consisting of 6×18 panels. Different time intervals (6 and 3 degrees) were employed to discretize the shed wake.

The discretization refinement for both the Euler grid and the vortex-lattice wake yields very small variations in the computed results [8]. Therefore, the "coarse" Euler grid has been employed in the present computations. The consistency of the results obtained by NUVOLA and ROSITA is demonstrated examining the load history and the vorticity fields, as in figure 2 where we superimposed the vortex lattice produced by a single blade predicted by NUVOLA and the isosurfaces of the vorticity vector modulus generated by ROSITA for the same azimuthal angle.

4 Discussion of results

Results will be presented in three subsections with different goals. In the first subsection, an extensive comparison with other single-blade and multi-blade codes is performed for the high speed case TC1 to assess the accuracy of the present results. Then,

		TC1 Modane 0987	TC2 HELISHAPE 0067	TC3 HELISHAPE 0165
Tip Mach number	M_{tip}	0.617	0.616	0.618
Advance ratio	μ	0.419	0.167	0.214
Shaft angle	α_{TPP}	11.8°	1.48°	−3.72°

Table 1: Flight conditions for the selected test cases

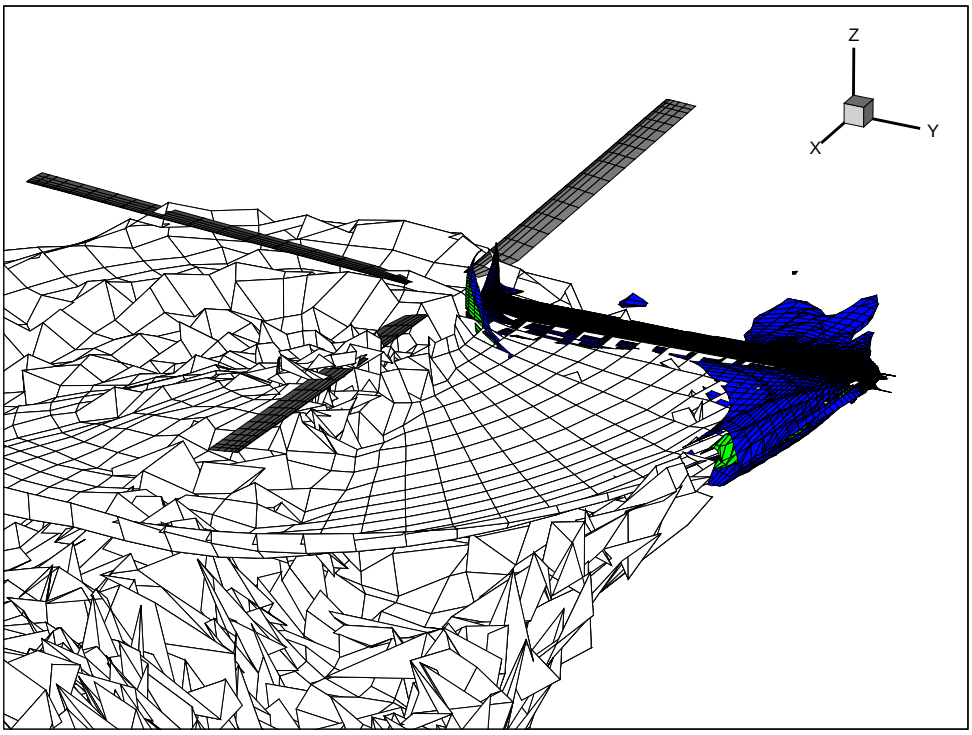

Figure 2: Wake system at $\Psi = 90°$ for TC2.

the effect of the vorticity confinement technique on the achieved results will be discussed for the two low speed test cases. Finally, a comparison between single-blade and Chimera results for TC3 will assess the efficiency of the single-blade approach.

4.1 Comparison with other codes

An assessment of the present results is carried out against experimental data and results from other codes. Test case TC1 has been selected because it has been computed by several authors with different methods [4], [19], [20]. The azimuthal variation of pitch angle θ (referred to $r/R = 0.7$) and flap angle β is specified as [20]:

$$\begin{aligned} \theta &= 11.36° + 1.9181° cos(\Psi) - 5.0778° sin(\Psi) \\ \beta &= 2.203° - 5.0778° cos(\Psi) \end{aligned}$$

while lag motion is neglected.

Figure 3 shows the temporal history of the blade normal force coefficient $C_n M^2$ at two spanwise stations ($r/R = 0.7$ and $r/R = 0.915$) obtained with the present method, together with those achieved by other single-blade approaches and with experiments. The other considered approaches are a full potential model (the common European code HeliFP [21]) and an Euler model (the DLR code ROTCATS [20]), both accounting for the wake influence through a modification of the solid body boundary conditions. The present results are close to those of the other single-blade methods, generally predicting lower loads at the different blade stations. The agreement between the three predictions and the experimental data may be considered of the same order of magnitude.

A similar comparison is made in figure 4 with the results obtained for multi-blade calculations [4], in which the wake is obtained as part of the Euler solution. The reference numerical results are obtained, respectively, with the ONERA moving blade method and with the DLR Chimera code. The agreement of the present single-blade calcula-

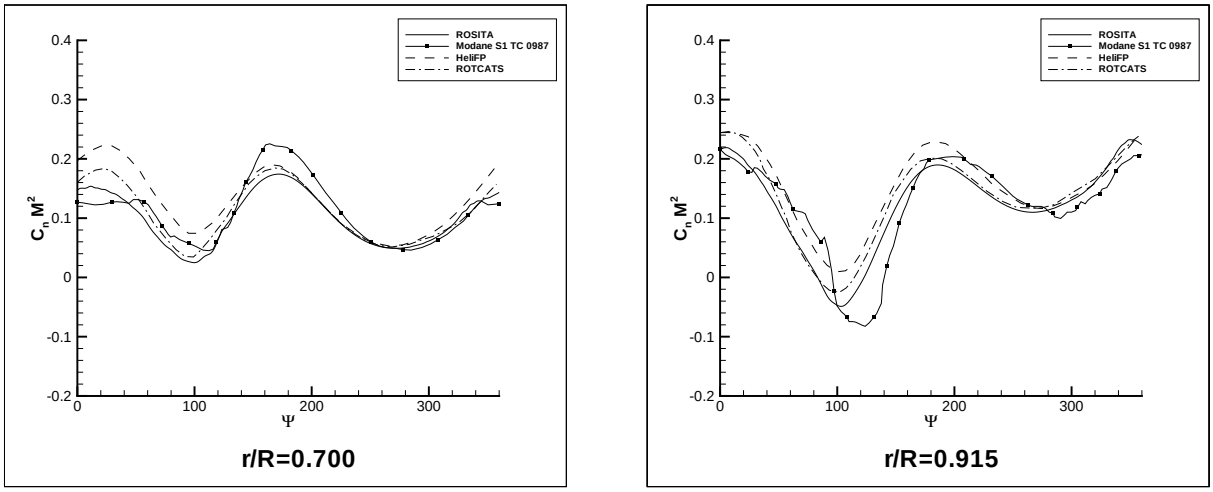

Figure 3: Comparison with other single-blade codes for TC1.

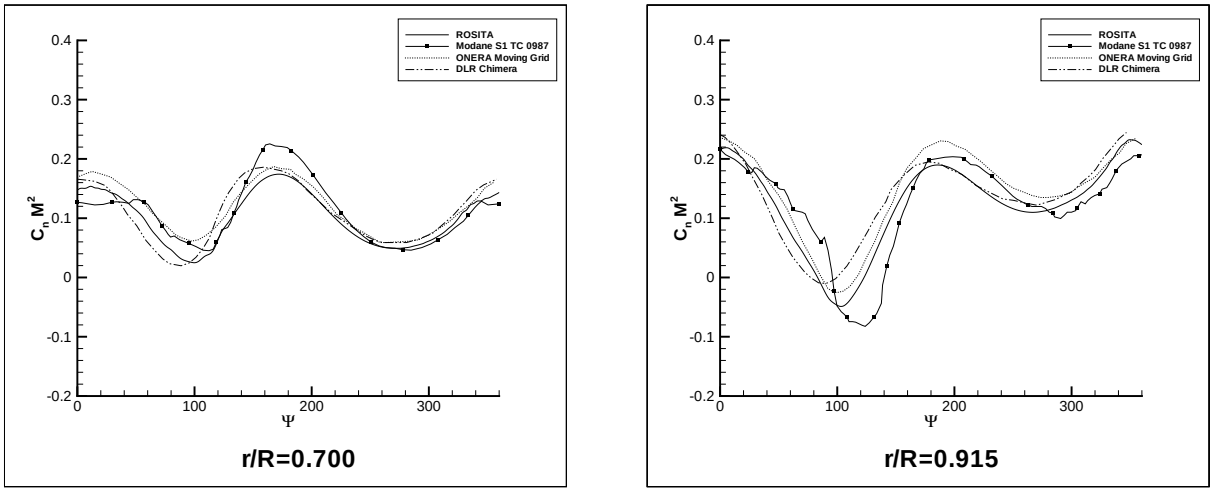

Figure 4: Comparison with multi-blade codes for TC1.

tions and the multi-blade approaches is encouraging, the differences between the numerical results being smaller than those observed with the previously examined single-blade methods.

4.2 Effects of vorticity confinement

An extensive set of calculations were carried out for TC2 to analyze the effects of the coefficient ϵ_c of the vorticity confinement model. Figure 5 reports the temporal history of the normal force coefficient C_n at two spanwise stations ($r/R = 0.5$ and $r/R = 0.7$), for values of ϵ_c ranging from zero to 3. The case without vorticity confinement ($\epsilon_c = 0$) is shown with the solid line. The overall influence of the confinement on the blade loads is small. It is more pronounced for the retreating blade ($240° < \Psi < 340°$) and mainly at the inboard station ($r/R = 0.5$).

The analysis of the vorticity field at $\Psi = 270°$ (fig. 6) clearly shows two effects influencing the loads. The tip vortex of the preceding blade, entering the domain through the imposed far-field boundary conditions, without vorticity confinement is quickly diffused. With confinement the vortex extends above the blade and its suction promotes a localized increase of the sectional loads at the outer ($r/R > 0.8$) blade stations. More inboard the confinement allow to reproduce the influence of the vortex sheets shed by the other blades, which interact in a quite complicated manner close to the rotor disk. The influence on the loads is clearly seen at $r/R = 0.5$, where the solutions with a sufficient amount of confinement better reproduce the waving distribution of C_n with azimuth.

There is a range of ϵ_c in which the result are unaf-

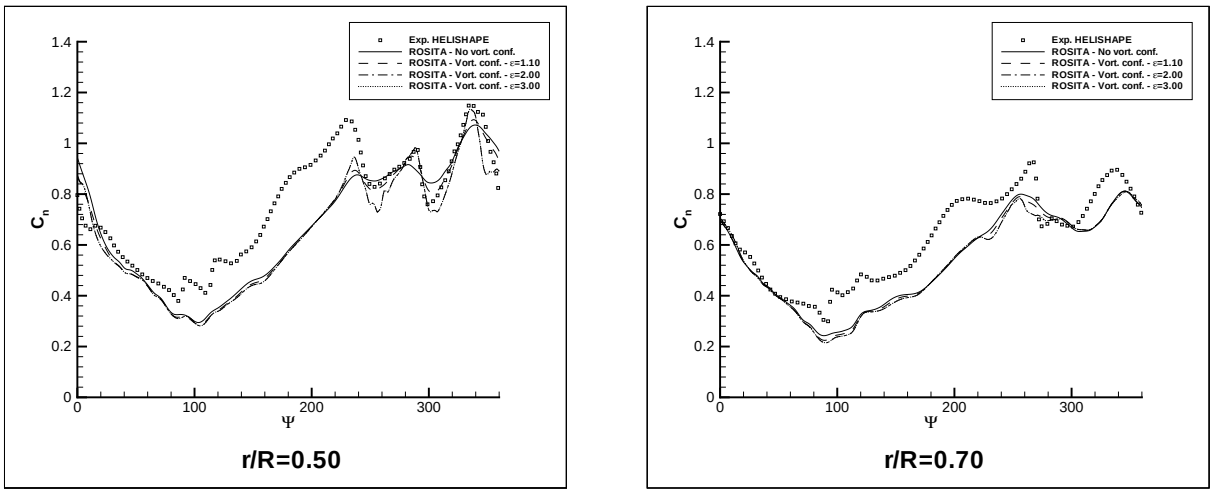

Figure 5: Effects of vorticity confinement on the computed load histories for TC2.

ϵ_c	C_T/σ
0.0	0.07301
0.1	0.07300
0.3	0.07297
0.9	0.07241
1.1	0.07228
2.0	0.07227
3.0	0.07227

Table 2: Overall thrust as function of the ϵ_c value for TC2.

fected by its particular value. In the results of fig. 5 the curves for $\epsilon_c = 2$ and $\epsilon_c = 3$ practically coincide. For a value of $\epsilon_c > 3.6$ it was not possible to reach a pseudo-time converged solution anymore. This suggests that a quantitative convergence of the results to the variation of ϵ_c should be sought by a trial and error procedure. The influence of the confinement technique on the overall thrust is anyway as small as 1% for the present case, as shown in Table 2.

The last considered test case, TC3, is characterized by a negative shaft angle (i.e. the shaft was inclined backward during wind tunnel tests). This configuration generally leads to the highest level of blade-vortex interaction and, consequently, is deemed particularly interesting to further assess the capabilities of the vorticity confinement method.

In figure 7 the temporal history of the normal force coefficient C_n for radial stations at $r/R = 0.70$ and $r/R = 0.82$ is shown, where the squares represent the experimental data and the solid line refers to the computation without vorticity confinement. Marked oscillations of the normal force coefficient may be observed in the experimental load history for azimuthal angles in the range $0 - 80°$ and $280 - 360°$, revealing, as expected, a close interaction between the blade and the wake system. The solution computed with no confinement, on the other hand, exhibits only partially the load peaks induced by the BVI, due to the fast dissipation of the vorticity.

Applying the vorticity confinement with $\epsilon_c = 3.0$ allows to achieve a closer matching between the computed normal force coefficient and the experimental, proving the effectiveness of the present approach. Nevertheless, some details of the experimental solution are still not well reproduced, even if values of the confinement parameter higher than 3.00 are used. As for TC2, the influence of ϵ_c on thrust is very small, being the improvement in C_T/σ lower than 0.6%.

4.3 Efficiency of the single-blade approach

To quantify the efficiency of the single-blade approach, a comparison is made for TC3 with a Chimera multi-blade calculation. The Chimera method developed during the EROS project [5] has been improved in the ROSITA code through a parallelization of the tagging process, needed to compute the connectivity of the overset grid system. The tagging algorithm in itself is very difficult to parallelize efficiently, requiring a large amount of inter-grid communications. An easy way to circumvent this difficulty is to perform the tagging calculations at the preprocessor stage for the whole rotor revolution, subdividing the different blade azimuthal positions among the processors. In this way the original tagging algorithm is retained, at the

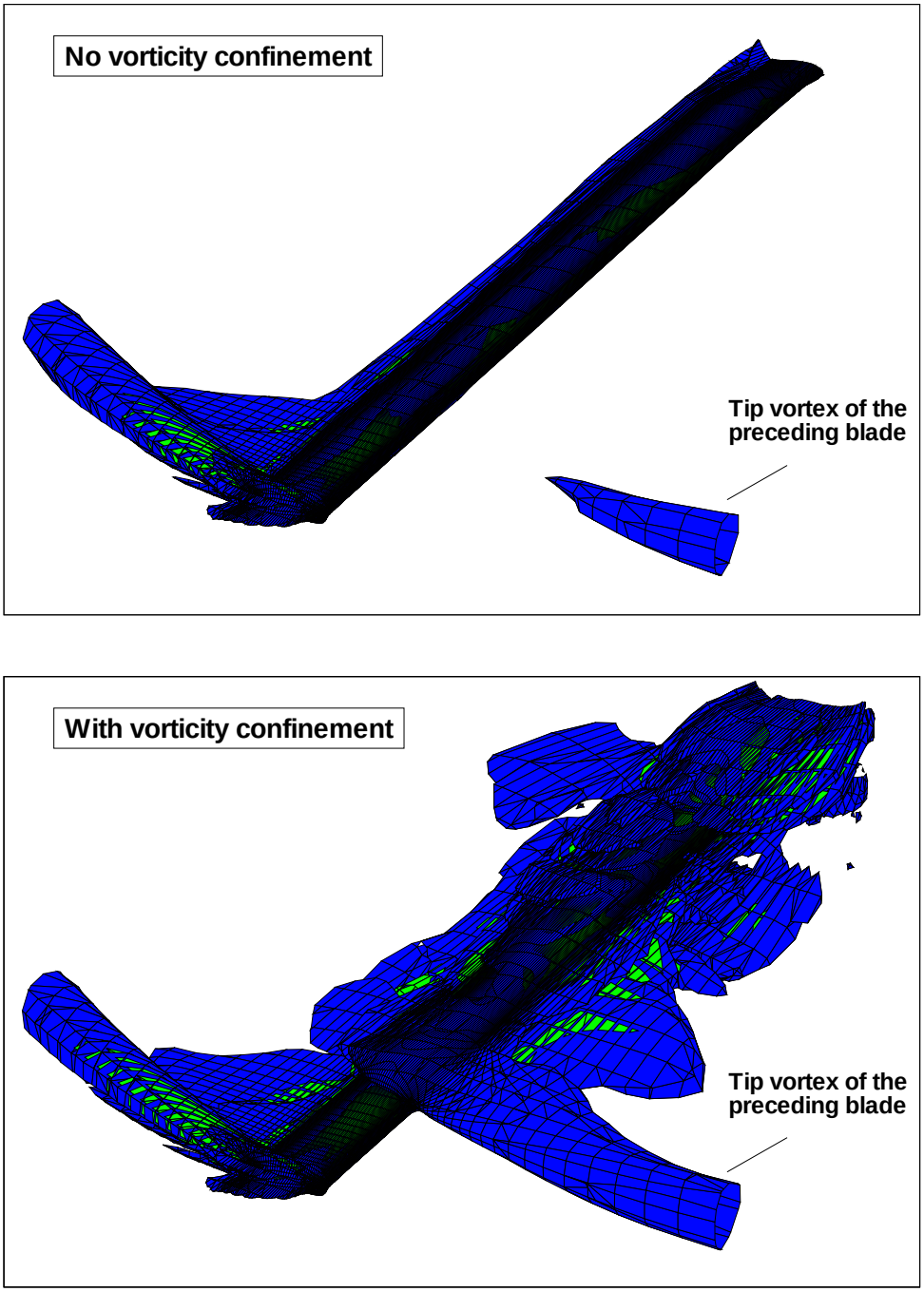

Figure 6: Isosurfaces of $|\omega| = 0.4$ without and with confinement at $\Psi = 270°$ for TC2.

mere expense of an increased disk space requirement.

The Chimera grid set employed is made of a $60 \times 50 \times 20$ cell grid for each of the four blades and of a $210 \times 66 \times 108$ cell background cylindrical grid (fig. 8), for a total of 1.73 million of unknowns, i.e. a rather coarse grid for both the blade and the wake regions. Computed results after two rotor revolutions, shown in figure 9 with the solid line, confirm that the grid is too coarse to correctly reproduce the blade-vortex interactions. Slightly better results are achieved with the single-blade calculations. The latter approach is obviously more computationally efficient, allowing for a seven-fold saving in CPU time for parallel runs on 10 processors, despite to the fact that the vortex lattice wake calculation has not been parallelized yet.

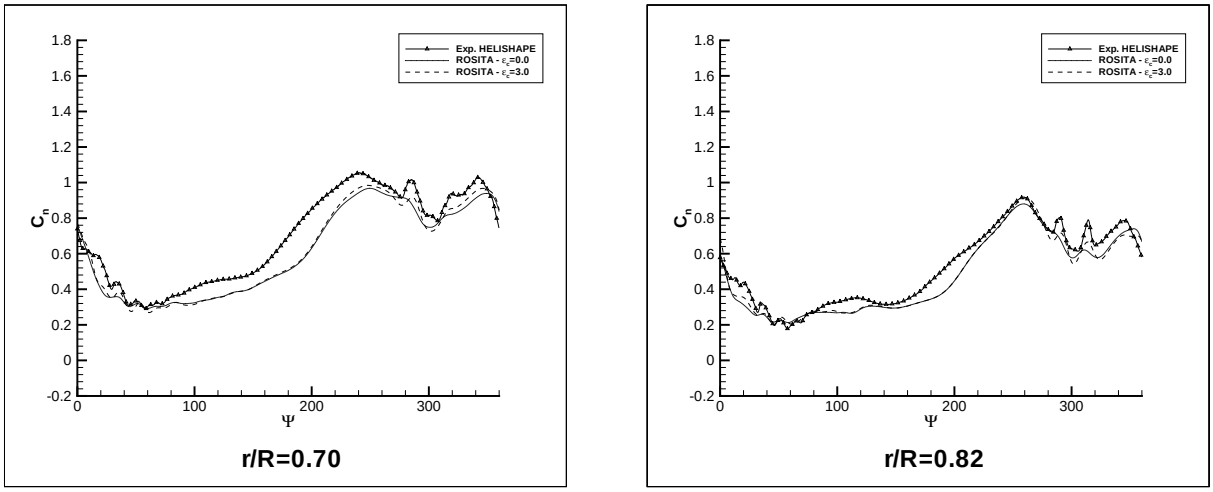

Figure 7: Effects of vorticity confinement on the computed load histories for TC3.

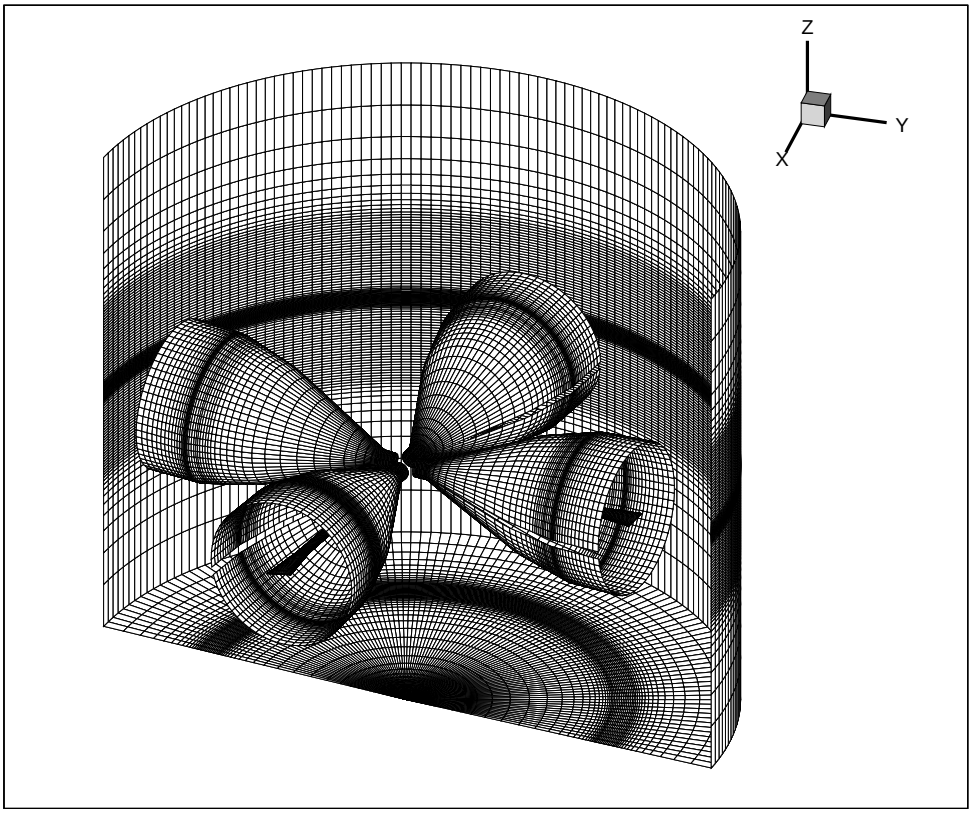

Figure 8: Chimera grid set for TC3.

5 Conclusions

Load predictions obtained with the ROSITA code, operating in single-blade mode, have been presented for the 7A and 7AD model rotors in high-speed and low-speed forward flight. Comparisons with experiments and with results from different numerical methods are encouraging. Despite the inherent theoretical discrepancy of its linear/non-linear coupling, the single-blade approach is shown to yield satisfactory results even in presence of moderate Blade Vortex Interaction (BVI) conditions. The agreement achieved by the present method with the experimental data is comparable with that of full-rotor simulations, at a much reduced computational effort. The achieved results demonstrate that forward flight aerodynamic performances may be computed in a very efficient way by a single grid near-field Euler computation in which the far-field

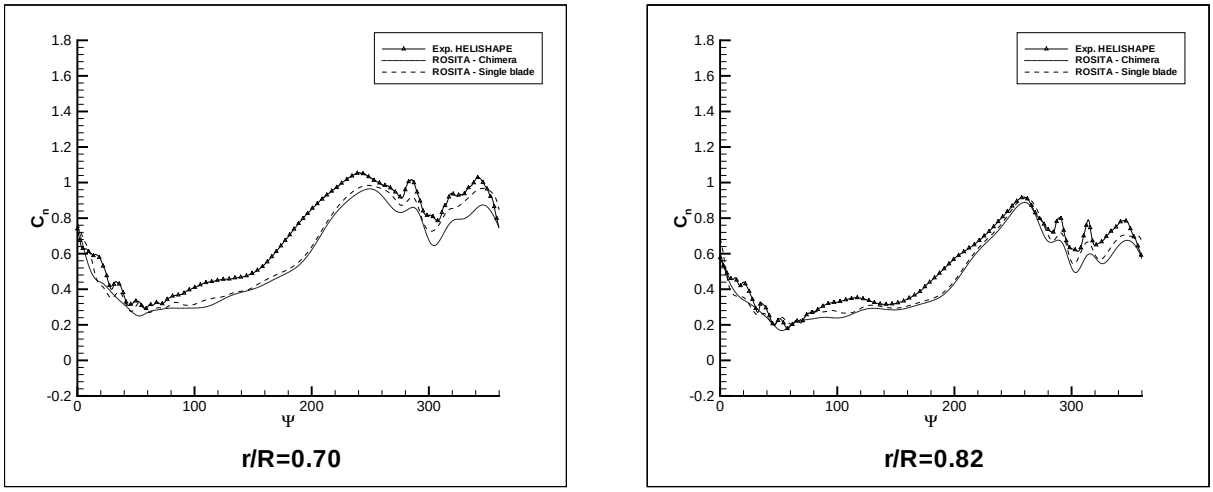

Figure 9: Comparison between Chimera and single-blade results for TC3

boundary conditions account for the presence of the full vortical wake, the latter being obtained with a free-wake vortex lattice method. The flexibility and efficiency of the present approach make it suitable for the simulation of manouvering flight and for the coupling with a rotor dynamic model, towards a fully integrated rotor performances prediction capability.

Acknowledgements

The work of the first and last Authors has been supported by Agusta under the contract 01/172/VIL.

References

[1] Meakin R.L. (1993). Moving Body Overset Grid Methods for Complete Aircraft Tiltrotor Simulations, 11^th AIAA Computational Fluid Dynamics Conference, Orlando, FL, AIAA 93-3350.

[2] Ahmad J., Duque E.P.N. (1994). Helicopter Rotor Blade Computation in Unsteady Flows Using Moving Overset Grids, 12^th AIAA Applied Aerodynamics Conference, Colorado Springs, CO, AIAA 94-1928.

[3] Stangl R., Wagner S. (1996). Euler Simulations of a Helicopter Configuration in Forward Flight Using a Chimera Technique, 52^nd American Helicopter Society Annual Forum, Washington D.C.

[4] Boniface J.-C., Pahlke K. (1996). Calculations of Multibladed Rotors in Forword Flight using 3D Euler Methods at DLR and ONERA, 22^nd European Rotorcraft Forum, Brighton, UK.

[5] Renzoni P., D'Alascio A., Kroll N., Peshkin D., Hounjet M.H.L., Boniface J.-C., Vigevano L., Allen C.B., Badcock K., Mottura L., Schoell E., Kokkalis A. (2000). EROS - a common European Euler code for the analysis of the helicopter rotor flowfield, *Progress in Aerospace Sciences*, **36**, 437-485.

[6] Wher D., Zerle L., Wagner S. (1996). Coupling Euler and Potential Methods for the Calculations of Helicopter Rotors in Unsteady Forword Flight, 22^nd European Rotorcraft Forum, Brighton, UK.

[7] Algermissen G., Wagner S. (1998). Computation of Helicopter BVI Noise by Coupling Free-Wake, Euler and Kirchhoff Method, AIAA Paper 98-2238.

[8] Biava M., Bindolino G., Vigevano L. (2003). Single Blade Computations of Helicopter Rotors in Forward Flight, 41^st AIAA Aerospace Sciences Meeting and Exhibit, Reno, NV, AIAA 2003-0052.

[9] Roe P.L. (1981). Approximate Riemann Solvers, Parameter Vectors and Difference Schemes, *Journal of Computational Physics*, **43**, 357-372.

[10] van Leer B. (1977). Towards the ultimate conservative difference scheme. IV. A new approach to numerical convection. *Journal of Computational Physics*, **23**, 276-299.

[11] Biava M., Vigevano L. (2002). The effect of far-field boundary conditions on tip vortex path predictions in hovering, CEAS Aerospace

Aerodynamics Research Conference, Cambridge, UK.

[12] Venkatakrishnan V. (1993). On the accuracy of limiters and convergence to steady state solutions, 31^{st} AIAA Aerospace Sciences Meeting and Exhibit, AIAA 93-0880, Reno, NV.

[13] Jameson A. (1991). Time Dependent Calculations Using Multigrid with Applications to Unsteady Flows past Airfoils and Wings, 10^{th} AIAA Computational Fluid Dynamics Conference, Honolulu, HI, AIAA 91-1596.

[14] Badcock K.K., Richards B.E. (1996). Implicit time stepping methods for the Navier-Stokes equations, *AIAA J.*, **34**, 555-559.

[15] Baron A., Boffadossi M. (1991). Numerical Simulation of Unsteady Rotor Wakes, 17^{th} European Rotorcraft Forum, Berlin, Germany.

[16] Hu G., Grossman B., Steinhoff J. (2000). A Numerical Method for Vortex Confinement in Compressible Flow, AIAA Paper 2000-0282.

[17] Biava M., Vigevano L. (2003). Assessment of the vorticity confinement technique applied to rotorcraft flows, 21^{st} AIAA Applied Aerodynamics Conference, Orlando, FL, AIAA 2003-3524.

[18] Schultz K.-J., Splettoesser W., Junker B., Wagner W., Schoell E., Arnaud G., Merker E., Pengel K., Fertis D. (1996). A parametric wind tunnel test on rotorcraft aerodynamics and aeroacoustics (HELISHAPE) - test procedures and representative results, 22^{nd} European Rotorcraft Forum, Brighton, UK.

[19] Beaumier P., Costes M., Gaveriaux R. (1993). Comparison beetween FP3D Full Potential Calculations and S1 Modane Wind Tunnel Test Results on Advanced Fully Instrumented Rotors, 19^{th} European Rotorcraft Forum, Cernobbio (Como), Italy.

[20] Schwarz T. (1997). Numerical Calculation of the flow about Rotors in Hover and Forward Flight by Potential 3D Euler Methods, DLR report, unpublished.

[21] Costes M., Le Balleur J.C., Gasparini L., Vigevano L., Hounjet M.H.L., Kokkalis A., Miller J.V., Spruce M., Pagano A., Renzoni P., Rocchetto A., Toulmay F. (1997). Development of a Common European Unsteady Full Potential CFD COde for Helicopter Rotors in Hover and Forward Flight, 53^{rd} Annual Forum of the American Helicopter Society, Virginia Beach, VA.